Aerosol Optical Extinction during the Front Range Air Pollution and Photochemistry Éxperiment (FRAPPÉ) 2014 Summertime Field Campaign, Colorado U.S.A.

Justin H. Dingle[1], Kennedy Vu[1], Roya Bahreini[1,2], Eric C. Apel [3], Teresa L. Campos[3], Frank Flocke[3], Alan Fried[4], Scott Herndon[5], Alan J. Hills [3], Rebecca S. Hornbrook [3], Greg Huey [6], Lisa Kaser [3], Denise D. Montzka[3], John B. Nowak[5], Mike Reeves[3], Dirk Richter[4], Joseph R. Roscioli[5], Stephen Shertz[3], Meghan Stell[3], David Tanner[6], Geoff Tyndall[3], James Walega [4], Petter Weibring[4], Andrew Weinheimer[3]

[1] Environmental Toxicology Graduate Program, University of California, Riverside, CA 92521
[2] Department of Environmental Sciences, University of California, Riverside, CA 92521
[3] National Center for Atmospheric Research, Boulder, CO 80301
[4] Institute for Arctic and Alpine Research, University of Colorado, Boulder, CO 80303
[5] Aerodyne Research, Inc., Billerica, MA 01821
[6] Department of Earth and Atmospheric Sciences, Georgia Institute of Technology, Atlanta, GA 30033

Corresponding author: R. Bahreini (roya.bahreini@ucr.edu)

Abstract. Summertime aerosol optical extinction (β_{ext}) was measured in the Colorado Front Range and Denver Metropolitan Area as part of the Front Range Air Pollution and Photochemistry Experiment (FRAPPÉ) campaign during July-August 2014. An Aerodyne Cavity Attenuated Phase Shift particle light extinction monitor (CAPS-PM$_{ex}$) was deployed to measure β_{ext} (at average relative humidity of 20 ±7%) of submicron aerosols at λ=632 nm at 1 Hz. Data from a suite of gas-phase instrumentation were used to interpret β_{ext} behavior under various categories of air masses and sources. Extinction enhancement ratios relative to CO ($\Delta\beta_{ext}/\Delta CO$) were higher in aged urban air masses compared to fresh air masses by ~50%. The resulting increase in $\Delta\beta_{ext}/\Delta CO$ under highly aged air masses was accompanied by formation of secondary organic aerosols (SOA). In addition, the impacts of aerosol composition on β_{ext} in air masses under the influence of urban, natural oil and gas operations (O&G), and agriculture and livestock operations were evaluated. Estimated non-refractory mass extinction efficiency (MEE) values for different air mass types ranged from 1.51-2.27 m^2 g^{-1}, with the minimum and maximum values observed in urban and agriculture influenced air masses, respectively. The mass distribution for organic, nitrate, and sulfate aerosols presented distinct profiles in different air mass types. During Aug. 11-12, regional influence of a biomass burning event was observed, increasing the background β_{ext} and estimated MEE values in the Front Range.

1 Introduction

Aerosol optical extinction coefficient (β_{ext}) represents the attenuation of light due to aerosol absorption and scattering of solar radiation. For a population of aerosol particles, β_{ext} depends on aerosol size, composition, particle number concentration, shape and morphology (Bohren and Huffman 1998). Atmospheric aerosols have important implications on climate. They modify the Earth's radiative energy budget directly through absorption and scattering of light, and indirectly through changing cloud characteristics (e.g., cloud droplet number concentration, cloud droplet size, cloud reflectivity, or lifetime) (Ramanathan et al. 2001, Seinfeld and Pandis 2006, Langridge et al. 2011). In addition, aerosols with diameters between 0.1 μm to 1 μm are the main contributors to visibility degradation in anthropogenically polluted areas and on regional scales due to their direct interactions with solar radiation (Malm 1989, Hobbs 2000, Ying et al. 2004). For example, it has been observed that the important anthropogenic contributors to light scattering in the Colorado Rocky Mountains are particulate matter from the urban emissions (Levin et al. 2009). The Denver Metropolitan area has also experienced seasonal air pollution and visibility degradation in the past. The wintertime pollution in Denver when trapped closer to the surface due to the low inversion layer causes a greyish-brown cloud referenced to as "Denver Brown Cloud." The composition of the Denver Brown Cloud and contribution of different chemical species to the observed β_{ext} during the wintertime have been investigated in 1970's to late 1980's (Groblicki et al. 1981, Wolff et al. 1981, Neff 1997). These studies concluded that among all the measured aerosol species, elemental carbon, ammonium sulfate, and ammonium nitrate contributed the most (37.7%, 20.2%, and 17.2 %, respectively) to wintertime optical extinction in the visible range. Previous measurements of summertime particle composition in the Colorado Front Range were conducted during the Northern Front Range Air Quality Study (NFRAQS) between July 17 to August 31, 1996 at several urban and rural sites. The major components of $PM_{2.5}$ mass were identified to be carbonaceous and inorganic aerosols, with carbonaceous aerosols contributing to about 46% of $PM_{2.5}$ mass. The 24-hour average measurements of $PM_{2.5}$ organic carbon, nitrate, and sulfate particles were observed to be 4.2 μg/m3, 0.9-1.2 μg/m3, and 1.4-1.5 μg/m3, respectively (Watson et al. 1998). In response to the wintertime haze episodes observed in the region, the State of Colorado has implemented a visibility standard based on total optical extinction of 76 Mm^{-1} at 550 nm, averaged during a 4-hr period when ambient RH is less than 70% (Ely et al. 1993). Total optical extinction measurements are provided by the Colorado Department of Public Health and Environment's transmissometer installed in Downtown Denver. The average total extinction values of August 2001-2014, ranging from 40-80 Mm^{-1}, reveal no significant trend in summertime extinction and visibility in the region since 2001.

The meteorological influence on air quality and visibility in the Front Range can also be important (e.g., Vu et al. 2016). Typically during the day, easterly upslope flow transports emissions from local sources westward while during the night, the flow reverses and downslope drainage flow through Platte River Valley sets in. Occasionally, a synoptic scale cyclone, called the Denver Cyclone, is established when drainage flow of air masses is prevented due to propagation of a vortex that develops east of the Rocky Mountains, contributing to transport and mixing of air masses in a cyclonic flow pattern (Crook et al. 1990, Reddy et al. 1995).

With a twofold increase in natural resource extraction wells since 2005 to about 24,000 active oil and natural gas (O&G) production wells in 2012, northeastern Colorado has experienced extensive fossil fuel production within the past decade (Scamehorn 2002, Pétron et al. 2014). This includes increases in fossil fuel production from coal bed methane, tight sand and shale natural gas, shale oil, and the associated gases. The emissions from these processes have several
5 environmental impacts such as greenhouse emissions of methane and emissions of non-methane hydrocarbons that impair air quality. Emissions from diesel trucks, drilling rigs, power generators, phase separators, dehydrators, storage tanks, compressors and pipes used in O&G operations also contribute to the regional burden of volatile organic compounds (VOCs), nitrogen oxides, and particulate matter (i.e., black carbon and primary organic carbon) (Gilman et al. 2013). One of the major air quality issues the Colorado Front Range faces is the exceedance of the 8-hour National Ambient Air Quality
10 Standard (NAAQS) standard for ozone (75 ppbv) during the summertime. In 2007, the Denver metropolitan area and the northern parts of the Colorado Front Range were classified as nonattainment areas due to the summertime elevated levels of ozone (www.colorado.gov/cdphe/attainment). Summertime impacts of O&G emissions on the formation of secondary pollutants and visibility reduction in the Front Range have not been explored previously. In addition to local point and area sources in the Front Range, biomass burning emissions from wildfires in the region may also act as a source of aerosols,
15 contributing to regional haze (Park et al. 2003).

During July-August 2014, airborne measurements were conducted over the Colorado Front Range as part of the Front Range Air Pollution and Photochemistry Éxperiment (FRAPPÉ) to characterize the influence of sources, photochemical processing, and transport on atmospheric gaseous and aerosol pollutants in the area. This paper will discuss the role of local aerosol sources in the Front Range and regional wildfires on aerosol optical extinction in the absence of the
20 Denver Cyclone by investigating chemical and optical properties of aerosols in different air masses.

2 Measurements

2.1 FRAPPÉ Field Campaign

In-situ measurements were conducted aboard the National Science Foundation/National Center for Atmospheric Research (NSF/NCAR) C-130 aircraft during July 20-August 18, 2014. Flight tracks of the C-130, color coded with different trace
25 gases, are presented in Figure 1a-c. In the current analysis, airborne data were limited to those obtained only in the boundary layer of the Colorado Front Range (i.e., altitudes below 2500 m above sea level (ASL) east of the foothills and below 5500 m ASL with easterly winds over the foothills and the Continental Divide) to capture the influence of local sources such as power plants, O&G, agriculture, livestock, and urban emissions. Occasionally, when air masses with the mountain-valley circulation patterns were sampled, data from higher altitudes (< 4000 m ASL) over the Denver Metropolitan area were also
30 considered.

2.2 Instrumentation and Methodology

The NSF/NCAR C-130 aircraft carried an extensive collection of instruments for the characterization of the diverse atmospheric pollutants in the Colorado Front Range. The relevant instrumentations used in the current analysis are described below. (The data produced by these instruments are available at http://www-air.larc.nasa.gov/cgi-bin/ArcView/discover-aq.co-2014?C130=1).

The extinction coefficient (β_{ext}) at 632 nm was measured using a Cavity Attenuated Phase Shift particle light extinction monitor (CAPS-PM$_{ex}$) (Aerodyne Research Inc., Billerica, MA). The CAPS-PM$_{ex}$, utilizes high reflectivity mirrors at two ends of a 26-cm long, near-confocal cavity. Within the optical cell cavity, the highly reflective mirrors create an effective path length of approximately 2 km. Under the particle free sampling mode, the light emitting diode (LED) light output is directed to the first mirror, while a small fraction passes through the second mirror to the photodiode detector, producing a slightly distorted waveform of the square-wave modulated by the LED, whereas under the aerosol sampling mode, the detector detects a greater distorted waveform, characterized by a phase shift. The vacuum photodiode, which is located behind the second reflective mirror detects and measures that phase shift when the square wave becomes distorted due to interactions with sampled air under a relatively long effective pathlength. The observed phase shift is then related to aerosol β_{ext} as follows:

$$\beta_{ext} = (\cot\theta - \cot\theta_o) * (2\pi f/c), \tag{1}$$

where $\cot\theta_o$ is the phase shift from the particle-free sampling mode, $\cot\theta$ is the phase shift during the aerosol sampling mode, f is the frequency, and c is the speed of light. The estimated uncertainty in β_{ext} is 10%, while the 3-σ detection limit for 1-s data under particle free air for the conditions encountered during FRAPPE was ~1.5 Mm^{-1} (Massoli et al. 2010, Petzold et al. 2013). Measurements of the baseline were conducted through the system's internal filter unit regularly, at 5 minute intervals. The filter period, which lasted for 1 minute, included 10 s of flush time, 40 s of filter sampling, followed by another 10 s of flush time. Although for majority (72%) of the data, consecutive baseline values had shifted by less than 0.5 Mm^{-1}, baseline values were interpolated for a more accurate estimation of optical extinction. CAPS-PM$_{ex}$ data, obtained at 1 Hz, were averaged to aerosol mass spectrometer's averaging time of 15 s. The measured β_{ext} includes the combined effects of scattering and absorption of light by aerosols at 632 nm; given relatively high single scattering albedo values of aerosols downwind of urban environments (Langridge et al. 2012), β_{ext} is expected to be dominated by scattering coefficient. As discussed in Section 3.3 and 3.4, in urban- or biomass burning-influenced air masses, contribution of absorption by black carbon to β_{ext} could be more significant. It is worth mentioning that anthropogenic gases such as nitrogen dioxide have minimal effect on the measured β_{ext} at 632 nm since regular baseline corrections based on sampled filtered air were applied to the data. Given the average mixing ratio of NO_2, the parameterization by Groblicki et al. (1981) for estimating NO_2 absorption at 550 nm, and the factor of 10 smaller value of NO_2 absorption cross section at 632 nm compared to 550 nm

(Schneider et al. 1987), we estimated the average contribution of NO_2 absorption at 632 nm to be ~0.1 Mm^{-1}, indicating a minor contribution to total extinction at 632 nm.

The CAPS-PM_{ex} shared a common inlet with a compact Aerosol Mass Spectrometer (mAMS; Aerodyne Inc., Billerica, MA) coupled with a time-of-flight (TOFwerk, Thun, Switzerland) detector to measure particle mass distribution and non-refractory submicron aerosol composition (NR-PM_1) of organics, nitrate, sulfate, chloride, and ammonium. The mAMS inlet was characterized to have a 50% transmission of ~800 nm (physical diameter) particles. Aerosol concentrations from the mAMS were corrected for vaporizer bounce using composition-dependent collection efficiencies (Middlebrook et al. 2012). The estimated uncertainty for all aerosol species is ~30% (Bahreini et al. 2009). Both instruments sampled particles through a secondary diffuser mounted inside a NCAR HIAPER modular inlet (HIMIL), mounted facing forward, under the C-130 aircraft. Given the total flow rate within the inlet and assuming particle density of 1500 kg/m^3, ambient temperature of 20 °C, and ambient pressure of 70 KPa, 2 μm particles were estimated to be transmitted by 50%, making the inlet nominally a PM_2 inlet. Residence time in the inlet was estimated to be ~0.56 s. Ambient aerosol size distributions were measured on-board the C-130 by a Passive Cavity Aerosol Spectrometer Probe (PCASP). Estimated extinction values using Mie calculations with a nominal refractive index of 1.5 and the measured PCASP size distributions indicated that particles smaller than 800 nm captured >92% of PM_2 extinction values, confirming that the majority of the extinction signal originated from aerosols in the size range of the mAMS. We note that the calculated extinction coefficients were not highly sensitive to the choice of refractive index; only a 4% decrease in the slope of scattering from $PM_{0.8}$ vs. PM_2 was observed by increasing the refractive index from 1.48 to 1.52.

Based on the ambient relative humidity (RH) and temperature and the temperature within the CAPS-PM_{ex} extinction cell, and assuming that aerosols had equilibrated to the conditions within the measurement cell, the CAPS-PM_{ex} measurements during the flights discussed here represent extinction values at an average RH of 20 ± 7 % (range of 15-30%). Additionally, β_{ext} values were normalized for STP (273 K and 1 atm) conditions..

The relationship between the primary emitted nitrogen oxides (NO_x) and the higher oxidized species of nitrogen captures the transformation of NO_x in the atmosphere upon aging (Kleinman et al. 2007, Langridge et al. 2012). Thus, measurements of nitric oxide (NO), nitrogen dioxide (NO_2), nitric acid (HNO_3), particulate phase nitrate (NO_3^-), alkyl nitrates (ANs), peroxy acetyl nitrate (PAN), and peroxy propionyl nitrate (PPN) were used to calculate the ratio of primary nitrogen oxides ($NO_x = NO + NO_2$) to NO_y ($NO_y = NO_x + HNO_3 + NO_3^- + ANs + PAN + PPN$) in order to track the extent of photochemical aging in an air mass with non-zero emissions of NO_x (Kleinman et al. 2007, DeCarlo et al. 2010). A ratio that yields a value close to one represents air masses that are relatively fresh whereas a ratio closer to zero represents more aged air mass. NO and NO_2 were measured using the NCAR 2-channel chemiluminescence instrument (Ridley and Grahek 1990). A chemical ionization mass spectrometer (CIMS) coupled with a quadrupole detector was operated to measure HNO_3, using SF_5^- as the reagent ion (Huey et al. 1998, Huey 2007). ANs were measured using thermal dissociation-laser induced fluorescence (TD-LIF) (Thornton et al. 2000, Day et al. 2002). PAN and PPN species were measured using the NCAR PAN-CIGAR CIMS (Slusher et al. 2004, Zheng et al. 2011), with I^- as the reagent ion.

The impacts of different pollution sources on sampled air masses were characterized by considering several auxiliary gas-phase tracers. Carbon monoxide, the tracer for combustion emissions, was measured by VUV-fluorescence with the estimated uncertainty of 3% (Gerbig et al. 1999). Ethane (C_2H_6), used to identify influence of O&G emissions, was measured using the Compact Atmospheric Multi-species Spectrometer (CAMS), employing infrared spectrometry (Richter et al. 2015). The Aerodyne dual quantum cascade trace gas monitor for ammonia (NH_3) equipped with a mid-infrared absorption spectrometer was used to identify emissions of agriculture and livestock operations (Ellis et al. 2010). The influence of biomass burning was identified using the measurements of hydrogen cyanide from the NCAR Trace Organic Gas Analyzer (TOGA), a fast gas chromatography coupled with a quadrupole mass spectrometer (GC-MS) set to selected ion monitoring mode for quantification (Apel et al. 2015) and acetonitrile by proton-transfer reaction mass spectrometry (PTR-MS), a high sensitivity instrument with fast time response that employs a quadrupole mass spectrometer to measure volatile organic compounds (de Gouw and Warneke 2007, Karl et al. 2009). A Passive Cavity Aerosol Spectrometer Probe (PCASP) was available as the only instrument to measure ambient aerosol size distributions in the size range of 0.1-3 µm (Rosenberg et al. 2012).

3. Results and Discussion

3.1 Urban Aerosol optical extinction characterization under different photochemical aging regimes

NO_x/NO_y ratios were observed to be highest over the city representing freshly emitted plumes from vehicular traffic (Figure S1). Away from the city center, NO_x/NO_y values decrease, representing the relative evolution of fresh air masses containing NO_x. Figure 2 shows the scatter plot of β_{ext} vs. CO, color coded with the NO_x/NO_y ratio, on August 2-3, 7-8, 15-16, 18 (i.e., excluding days with the influences of the Denver Cyclone and biomass burning events). Measurements here focused on air masses impacted by urban sources only, as defined by enhancement of CO over the background (105 ppbv, as defined by the mode in the frequency distribution of CO in the Front Range boundary layer) while $\Delta C_2H_6/\Delta CO < 20$ pptv ppbv^{-1} (Warneke et al. 2007, Borbon et al. 2013). The extinction enhancement ratios $\Delta\beta_{ext}/\Delta CO$ under 2 aging regimes, categorized by NO_x/NO_y ratio values, were analyzed by weighted linear orthogonal distance regression (ODR) fits, with the slopes representing the enhancement ratios. In obtaining these fits, weights represented standard deviations equal to the uncertainties in CO (3%) and β_{ext} (10%). Uncertainties in the slope values of ODR fits throughout the manuscript represent the estimated propagated uncertainties, in this case the square-root of the quadratic sum of the relative uncertainties in the ODR fit (1-σ), CO mixing ratio, and β_{ext} coefficient. NO_x/NO_y values of <0.5, and > 0.5 represent relatively aged and fresh NO_x-containing air masses, respectively. Different trends in $\Delta\beta_{ext}/\Delta CO$ were seen under the two aging regimes, with a lower value of 0.13 ± 0.014 Mm^{-1} ppbv^{-1} observed in the fresh air masses. On the other hand, the relatively aged air masses showed a higher $\Delta\beta_{ext}/\Delta CO$ value of 0.20 ± 0.025 Mm^{-1} ppbv^{-1}, indicating about a 54% increase in the extinction enhancement ratio due to photochemical aging. The correlation coefficient r values were 0.92 and 0.85 for relatively fresh and aged air masses, respectively. The most dominant component of the non-refractory aerosols in urban plumes was OA, with a 74 %

contribution to NR-PM$_1$ mass. The high OA contribution combined with the observed significant increase in the enhancement ratio of OA to CO with aging (from 0.021 ± 0.009 µg m^{-3} ppbv^{-1} to 0.11 ± 0.01 µg m^{-3} ppbv^{-1}) suggest that the bulk of the aged urban aerosol mass during the daytime in the Front Range was SOA. Since $\Delta NO_3^-/\Delta CO$ and $\Delta SO_4^{2-}/\Delta CO$ enhancement ratios did not increase with photochemical aging and demonstrated poor overall correlation coefficients (r <0.35 for $\Delta NO_3^-/\Delta CO$ and r <0.29 for $\Delta SO_4^{2-}/\Delta CO$), the increase in the enhancement ratio of aerosol optical extinction coefficient with CO was likely also driven by SOA formation.

3.2 Impacts of source and aerosol composition on aerosol optical extinction

Analysis of the average composition of NR-PM$_1$ in the Northern Front Range, in the absence of the Denver Cyclone, revealed significantly higher concentrations of organic aerosols relative to inorganic anions in the urban- and urban + O&G-influenced air masses, with a fractional contribution of ~74% (Figure 3).. On average, similar concentrations of non-refractory aerosol sulfate and chloride were observed in the different air masses while concentration of nitrate aerosols increased by a factor of ~2-3 in agriculturally-influenced air masses compared to the other air mass types with the exception of urban+O&G air masses.

Aerosol optical extinction values under the influence of different sources were further analyzed using auxiliary gas-phase data. As mentioned in Section 3.1., urban emissions were classified by enhancement of CO over the background (105 ppbv, as defined by the mode in the frequency distribution of CO in the Front Range boundary layer) while $\Delta C_2H_6/\Delta CO < 20$ pptv ppbv^{-1}. O&G and agricultural emissions were classified using enhancements of C$_2$H$_6$ over 2500 pptv, and that of ammonia over 5 ppbv, respectively, when all other tracers were at background level. A fourth air mass classification used in this analysis, urban + O&G, was based on air masses where both urban and O&G classifications were satisfied. The background mixing ratios for each gas tracer were determined by the mode of the frequency distribution of the tracer's mixing ratio observed in each flight. The impacts of sources and aerosol composition on extinction were explored by considering correlation coefficients of linear least-squared regression fits to the scatter plots of aerosol extinction vs. the mass concentration of the three dominant aerosol species (OA, nitrate aerosols, and sulfate aerosols) in urban-, O&G-, urban + O&G, and agricultural-influenced air masses.

Figure 4 shows the correlation coefficient (r) values of extinction vs. aerosol species mass concentration, in different air mass types as characterized above. The scatter plots of β$_{ext}$ vs. OA under urban, O&G, and urban + O&G air masses presented correlation coefficients of r = 0.46, 0.72, 0.46, respectively. This observation suggests that O&G emissions are important for organic aerosol contribution to β$_{ext}$. On the other hand, in urban plumes, the correlation between β$_{ext}$ and OA was lower than in O&G plumes while as demonstrated in Figure 2, β$_{ext}$ and CO were strongly correlated under both fresh and aged air masses. These observations suggest that species other than OA, e.g., black carbon, that are co-emitted with CO are also important in driving β$_{ext}$ in urban-influenced air masses. . The correlation between β$_{ext}$ vs. OA was weakest in plumes with agricultural emissions (r = 0.085), suggesting OA had little impact on β$_{ext}$ in these plumes. The correlation coefficients for β$_{ext}$ vs. aerosol nitrate mass were strongest under the influence of O&G, urban+ O&G, and agriculture and livestock

emissions (r = 0.75, 0.75 and 0.90 respectively), and weakest in the urban plumes (r = 0.18). Aerosol nitrate formation depends on ambient conditions (temperature and relative humidity), relative mixing ratios of nitric acid and ammonia, as well as aerosol composition and pH (Seinfeld and Pandis 2006, Weber et al. 2016). With uniform concentrations of sulfate aerosol and small contribution of chloride and dust components to the Front Range fine aerosol mass, variability in aerosol pH was not expected to be high. Furthermore, there was no specific trend in temperature or relative humidity in different plume types. On the other hand, mixing ratios of ammonia were observed to be variable in the different air masses, with average values of 1.41 ± 1.2 ppbv, 2.75 ± 1.88 ppbv, 8.21 ± 2.06 ppbv, and 5.47 ± 1.81 ppbv in urban, O&G, agriculture, and urban+O&G plumes, respectively. These observations suggest that ammonia emissions that are co-located with O&G-related activities in the Front Range play a significant role in controlling β_{ext} in these air masses by enhancing the partitioning of nitric acid to the condensed phase. In fact, the average aerosol inorganic nitrate fraction over total inorganic nitrate (aerosol nitrate/ [HNO_3 + aerosol nitrate]) under agriculture and O&G plumes were 0.25 ± 0.09 and 0.11 ± 0.10, respectively, compared to 0.070 ± 0.071 in urban-influenced plumes. β_{ext} was poorly correlated with sulfate aerosols in the region under the influence from all sources (r = 0.30, 0.37, 0.07, 0.23 for urban, O&G, agriculture, and urban+O&G respectively), suggesting a low impact of sulfate aerosol and its precursors on β_{ext} in the region.

Due to the higher hygroscopicity of inorganic salts compared to organics, contribution of sulfate and nitrate aerosols to the ambient β_{ext} could be higher than what is discussed above. However, under the average ambient conditions encountered during FRAPPÉ (average RH ~44 ±17 %), the increase in ambient β_{ext} due to aerosol hygroscopicity is not expected to be significant (~20%) given the high organic fraction of 64-74% in urban-, O&G-, or urban + O&G-influenced plumes (Massoli et al. 2009). In agriculturally-influenced plumes, the influence of nitrate aerosol on ambient β_{ext} will be greater because of the lower organic fraction and higher nitrate mass in these plumes, re-emphasizing the role of nitrate aerosol on β_{ext} under such emissions.

3.3 Mass Extinction Efficiency

Mass extinction efficiency (MEE) is a function of the diameter of the particle, wavelength of attenuated light, and aerosol refractive index (Seinfeld and Pandis 2006). To further asses the impacts of aerosol sources on β_{ext}, MEE values, i.e., the ratio of the observed β_{ext} to NR-PM$_1$ mass, in different air masses were estimated. For this analysis, MEE values were determined as the slope of the weighted linear ODR fits of β_{ext} against NR-PM$_1$ mass, with weights representing standard deviations equal to the uncertainties in NR-PM$_1$ mass (30%) and β_{ext} (10%). As indicated in Figure 5a-d, MEE values under the urban, O&G, agriculture, and urban + O&G influence were ~ 1.51 ± 0.49 m^2 g^{-1} (r=0.40), 1.62 ± 0.51 m^2 g^{-1} (r=0.79), 2.27 ± 0.83 m^2 g^{-1} (r=0.83), and 2.14 ± 0.68 m^2 g^{-1} (r=0.73) , respectively. The highest average MEE value was observed in agricultural plumes although considering the uncertainties in the fitted slopes, the MEE values were not significantly different. The overall MEE value in the Front Range, i.e., MEE observed for aerosols in all air mass types but in the absence of biomass burning, was 2.24 ± 0.71 m^2 g^{-1} (r= 0.80). Based on the values of the intercepts of the ODR fits in Figure 5, it appears that at background levels of NR-PM$_1$ mass, there was a background extinction value of ~2 Mm^{-1} in all, except

agricultural, plumes. This observation could be explained by optical extinction due to presence of refractory aerosol species, such as black carbon or dust, which are not accounted for in NR-PM$_1$ mass. High degree of correlation between β$_{ext}$ and CO (Figure 2) in urban plumes and low average concentrations of some of the dust components (e.g., calcium and magnesium) throughout the region support the non-negligible contribution of BC to β$_{ext}$ in the Front Range.

As seen in Figure S2, different aerosol mass distributions were observed under different air mass types. For the mass distribution analysis, d_{va} (vacuum aerodynamic diameter) was converted to d_p (physical diameter) by dividing d_{va} by the overall mass-weighted effective density (ρ), assuming ρ=1.25 g cm^{-3} for OA, ρ =1.75 g cm^{-3} for ammonium sulfate and ammonium nitrate, and assuming that particles sampled by the mAMS were internally mixed (Jayne et al. 2000, Seinfeld and Pandis 2006). Next we examine the similarity of MEE values observed in the Colorado Front Range to previous measurements. MEE is the sum of the mass absorption and scattering efficiencies (MAE and MSE respectively), which both depend on particle size, refractive index, and wavelength of light (Seinfeld and Pandis 2006). For typical urban air masses, mass distributions were dominated by organic aerosols in the size range of d_p=150-500 nm (Figure S2a). This is consistent with previous observations for urban aerosol volume distributions with modes at the size range of d_p ~ 200-500 nm (Seinfeld and Pandis 2006). Under O&G air masses (Figure S2b), individual mass distributions were broader, with modes for all species shifted to larger sizes (d_p ~ 200-550 nm). In agriculturally-influenced air masses nitrate aerosols presented a significant mode in the size range of d_p ~ 250-400 nm while OA species were concentrated on smaller sizes (dp ~ 100-200 nm; Figure S2c). The mass distributions in urban + O&G plumes were more variable. Occasionally, the distribution was dominated by OA in the smaller size range (~ 90-110 nm), but it also included contributions from sulfates and nitrates in the larger size (~ 225-275 nm and ~ 430-550 nm) (Figure S2d) while other times the mass distribution had significantly higher contribution from OA in the size range of ~ 225-350 nm, showing a clear shift and OA growth to larger sizes (Figure S2e).

Keeping in mind that in the presence of absorbing species, MEE is higher than mass scattering efficiency (MSE), in the absence of estimates of MEE in other regions, we present estimates of MSE from previous studies for comparison with the current MEE estimates in the Front Range. PM$_{2.5}$ scattering efficiencies at 550 nm in several ground based studies in urban commercial/ residential sites have typically been measured to be in the range of 2-3 m^2 g^{-1} in (Chow et al. 2002, Hand and Malm 2007). In such studies, the main aerosol sources contributing to the observed PM$_1$ MSE were the automotive emissions and combustion processes. Although the contribution of elemental or black carbon to PM$_1$ mass during FRAPPE is unknown, similar to these previous studies, OA contributed the most to the NR-PM$_1$ mass in the Front Range and in comparison, the observed average MEE value (2.24 ± 0.71 m^2 g^{-1}) is consistent with the previous estimates of MSE.

3.4 Impacts of biomass burning (BB) emissions on optical extinction

During August 11 and 12, several wildfires were observed at Rocky Mountain National Park, near Tonahutu Creek Trail, 60 miles NW of Denver and Grand Mesa, Uncompahgre and Gunnison National Forest. BB gas-phase markers, namely hydrogen cyanide (HCN) and acetonitrile (CH$_3$CN) from TOGA and PTR-MS airborne data, respectively, were elevated in the boundary layer throughout the flights on Aug. 11-12 compared to non-biomass burning days (July 26, 29, 31 and August

2-3, 7-8, 15-16, 18). For example, during the BB days, HCN (CH$_3$CN) mean mixing ratio in the boundary layer was 516 ± 58 pptv (201 ± 44 pptv) whereas the boundary layer mean mixing ratio on non-BB days was 327 ± 59 pptv (148 ± 38 pptv). Since elevated levels of HCN and CH$_3$CN were not observed in individual plumes but rather throughout the boundary layer on Aug. 11-12, a regional influence of biomass burning emissions was suspected to be present in the Front Range during this time. In addition, a 25 ppbv increase in CO background values were observed on Aug. 11-12 (Figure S3) compared to non-BB days. Ground-based measurements of PM$_{2.5}$ from Denver-La Casa (39.78 N, -105.01W), Denver-CAMP (39.75 N, -104.99 W), and Denver-I25 (39.73 N, -105.02 W) sites were analyzed to assess the regional impact of wildfire emissions in the Front Range to PM$_{2.5}$ during the BB and non-BB days. The time series of PM$_{2.5}$ mass concentrations at the sites described above, during days preceding and following the wildfires show increases in mass concentration for PM$_{2.5}$ during the days of BB (Figure S4). The mean PM$_{2.5}$ mass concentrations during the times of 9 am to 7 pm local time at Denver, La Casa, Denver-CAMP, and Denver-I25 during non-BB days were 5.61 ± 2.02, 6.01 ± 3.52, and 7.28± 2.91µg m^{-3}, while mean mass concentrations increased to 9.47 ± 2.05, 11.51 ± 3.04, and 14.08 ± 4.68 µg m^{-3}, respectively, during the BB days. As seen in Figure 6, the average daytime PM$_{2.5}$ mass concentration on BB days increased by 75-98% compared to the non-BB days confirming the regional influence of wildfires on the Front Range aerosol loadings.

In addition to scattering of light by smoke particles, BB emissions of black carbon (BC) and brown carbon (BrC) can lead to significant absorption of the solar radiation in the visible and UV region; at 632 nm absorption by BrC is minimal (Lack et al. 2012, May et al. 2014). MEE values were analyzed for days with and without the BB influence, using weighted linear ODR fit analysis, as explained previously. As seen in Figure 7, average MEE on Aug. 11-12 was~ 63% greater compared to days without the influence of BB (3.65 ± 1.16 m^2 g^{-1} vs. 2.24 ± 0.71 m^2 g^{-1}). Additionally, during Aug. 11-12, background value of airborne β_{ext} was higher at 4.00 ± 0.71 Mm^{-1} compared to 0.25 ± 0.11 Mm^{-1} on days without the BB influence, suggesting the additional contribution to β_{ext} from the wildfires. Although the AMS does not detect refractory materials such as BC due to the relatively low temperature of its vaporizer (600 °C), it is likely that on Aug. 11-12, BC emissions from the fires had resulted in elevated extinction values on a regional scale, resulting in higher MEE. The observed increase in MEE on Aug. 11-12 suggest that regional BB emissions have at least a comparable impact on aerosol optical extinction and visibility in the Front Range relative to the local sources.

4 Conclusions

Airborne aerosol optical extinction (632 nm) and submicron non-refractory aerosol composition were measured during the summer in the Colorado Front Range to understand sources and processes that impact summertime visibility in the area. In assessing the role of atmospheric processing on β_{ext}, $\Delta\beta_{ext}/\Delta CO$ enhancement ratio increased under aged urban air masses by ~54%. The increase in $\Delta\beta_{ext}/\Delta CO$ in the aged air masses was accompanied by a factor of ~5 increase in $\Delta OA/\Delta CO$, indicating that secondary formation of organic aerosols had significant impacts on the evolution of urban β_{ext} in the Front Range. Correlation between β_{ext} vs organic, nitrate, and sulfate aerosol mass under urban, O&G, agriculture, and urban + O&G mixed source influence were analyzed by linear regression fits. β_{ext} best correlated with organic aerosols under the

O&G emissions and best correlated with nitrate aerosols under the O&G and agriculture influences. Correlation with sulfate was poor under all air mass types. Estimated average non-refractory mass extinction efficiency values for different air mass types ranged from 1.51 ± 0.49 m^2 g^{-1} to 2.27 ± 0.83 m^2 g^{-1}, with the minimum and maximum average values observed in urban and agriculture air masses, respectively. Finally, aerosol components emitted from wildfires during the days of August

5   11 and 12 increased β_{ext} background values by ~ 4 Mm^{-1} and resulted in higher average MEE values by about 63% compared to non-biomass burning days, indicating that summertime visibility in the Front Range may equally be impacted by regional wildfires in addition to local sources.

Acknowledgments

10   The authors thank Daniel Adams (UCR's CNAS Machine Shop) and technicians at the NCARs Research Aviation Facility for integration of the instruments on the aircraft rack, a smooth aircraft integration process, and support throughout the project, Joshua Schwarz (NOAA-ESRL) for providing us the aircraft inlet system, Ron Cohen and Carly Ebben for providing the TD-LIF data, the Colorado Department of Public Health and Environment for funding and ground-based PM data, as well as the *USDA National Institute of Food and Agriculture, Hatch project Accession No. 233133* for additional

15   funding support. Data used in this analysis may be obtained at http://www-air.larc.nasa.gov/cgi-bin/ArcView/discover-aq.co-2014?C130=1.

References

Apel, E. C., et al. (2015). "Upper tropospheric ozone production from lightning NOx-impacted convection: Smoke ingestion case study from the DC3 campaign." Journal of Geophysical Research-Atmospheres 120(6): 2505-2523.

5 Bahreini, R., et al. (2009). "Organic aerosol formation in urban and industrial plumes near Houston and Dallas, Texas." Journal of Geophysical Research-Atmospheres 114.

Bohren, C. F. and D. R. Huffman (1998). Absorption and Scattering of Light by Small Particles. New York, Wiley.

10 Borbon, A., et al. (2013). "Emission ratios of anthropogenic volatile organic compounds in northern mid-latitude megacities: Observations versus emission inventories in Los Angeles and Paris." Journal of Geophysical Research-Atmospheres 118(4): 2041-2057.

Chow, J. C., et al. (2002). "Comparability between PM2.5 and particle light scattering measurements." 15 Environmental Monitoring and Assessment 79(1): 29-45.

Crook, N. A., et al. (1990). "THE DENVER CYCLONE .1. GENERATION IN LOW FROUDE-NUMBER FLOW." Journal of the Atmospheric Sciences 47(23): 2725-2742.

20 Day, D. A., et al. (2002). "A thermal dissociation laser-induced fluorescence instrument for in situ detection of NO2, peroxy nitrates, alkyl nitrates, and HNO3." Journal of Geophysical Research-Atmospheres 107(D5-6).

de Gouw, J. and C. Warneke (2007). "Measurements of volatile organic compounds in the earths atmosphere using proton-transfer-reaction mass spectrometry." Mass Spectrometry Reviews 26(2): 223-257.

25

DeCarlo, P. F., et al. (2010). "Investigation of the sources and processing of organic aerosol over the Central Mexican Plateau from aircraft measurements during MILAGRO." Atmospheric Chemistry and Physics 10(12): 5257-5280.

Ellis, R. A., et al. (2010). "Characterizing a Quantum Cascade Tunable Infrared Laser Differential Absorption 30 Spectrometer (QC-TILDAS) for measurements of atmospheric ammonia." Atmospheric Measurement Techniques 3(2): 397-406.

Ely, D. W., et al. (1993). The establishment of the Denver visibility standard. Air And Waste Management Association Annual Meeting, Air And Waste Management Association. 1.

5   Gerbig, C., et al. (1999). "An improved fast-response vacuum-UV resonance fluorescence CO instrument." Journal of Geophysical Research-Atmospheres 104(D1): 1699-1704.

Gilman, J. B., et al. (2013). "Source Signature of Volatile Organic Compounds from Oil and Natural Gas Operations in Northeastern Colorado." Environmental Science & Technology 47 1297−1305.

Groblicki, P. J., et al. (1981). "VISIBILITY-REDUCING SPECIES IN THE DENVER BROWN CLOUD .1. RELATIONSHIPS BETWEEN EXTINCTION AND CHEMICAL-COMPOSITION." Atmospheric Environment 15(12): 2473-2484.

15   Hand, J. L. and W. C. Malm (2007). "Review of aerosol mass scattering efficiencies from ground-based measurements since 1990." Journal of Geophysical Research-Atmospheres 112(D18).

Hobbs, P. V. (2000). Introduction to Atmospheric Chemistry: A Companion Text to Basic Physical Chemistry for the Atmospheric Sciences. Cambridge, Cambridge UP.

Huey, L. G. (2007). "Measurement of trace atmospheric species by chemical ionization mass spectrometry: Speciation of reactive nitrogen and future directions." Mass Spectrometry Reviews 26(2): 166-184.

Huey, L. G., et al. (1998). "Fast time response measurements of HNO3 in air with a chemical ionization mass
25   spectrometer." Journal of Geophysical Research-Atmospheres 103(D3): 3355-3360.

Jayne, J. T., et al. (2000). "Development of an aerosol mass spectrometer for size and composition analysis of submicron particles." Aerosol Science and Technology 33(1-2): 49-70.

30   Karl, T., et al. (2009). "Emissions of volatile organic compounds inferred from airborne flux measurements over a mega city." Atmos. Chem. Phys. 9(1): 271-285.

Kleinman, L. I., et al. (2007). "Aircraft observations of aerosol composition and ageing in New England and Mid-Atlantic States during the summer 2002 New England Air Quality Study field campaign." Journal of Geophysical Research-Atmospheres 112(D9).

Lack, D. A., et al. (2012). "Brown carbon and internal mixing in biomass burning particles." Proc Natl Acad Sci U S A 109(37): 14802-14807.

Langridge, J. M., et al. (2012). "Evolution of aerosol properties impacting visibility and direct climate forcing in an ammonia-rich urban environment." Journal of Geophysical Research: Atmospheres 117(D21): n/a-n/a.

Langridge, J. M., et al. (2011). "Aircraft Instrument for Comprehensive Characterization of Aerosol Optical Properties, Part I: Wavelength-Dependent Optical Extinction and Its Relative Humidity Dependence Measured Using Cavity Ringdown Spectroscopy." Aerosol Science and Technology 45(11): 1305-1318.

Levin, E. J. T., et al. (2009). "Aerosol physical, chemical and optical properties during the Rocky Mountain Airborne Nitrogen and Sulfur study." Atmospheric Environment 43(11): 1932-1939.

Malm, W. C. (1989). "Atmospheric Haze-Its Sources and Effects on Visibility in Rural Areas of the Continental United States." Environmental Monitoring and Assessment 12(3): 203-225.

Massoli, P., et al. (2009). "Aerosol optical and hygroscopic properties during TexAQS-GoMACCS 2006 and their impact on aerosol direct radiative forcing." Journal of Geophysical Research-Atmospheres 114.

Massoli, P., et al. (2010). "Aerosol Light Extinction Measurements by Cavity Attenuated Phase Shift (CAPS) Spectroscopy: Laboratory Validation and Field Deployment of a Compact Aerosol Particle Extinction Monitor." Aerosol Science and Technology 44(6): 428-435.

May, A. A., et al. (2014). "Aerosol emissions from prescribed fires in the United States: A synthesis of laboratory and aircraft measurements." Journal of Geophysical Research-Atmospheres 119(20): 11826-11849.

Middlebrook, A. M., et al. (2012). "Evaluation of Composition-Dependent Collection Efficiencies for the Aerodyne Aerosol Mass Spectrometer using Field Data." Aerosol Science and Technology 46(3): 258-271.

Neff, W. D. (1997). "The Denver Brown Cloud studies from the perspective of model assessment needs and the role of meteorology." Journal of the Air & Waste Management Association 47(3): 269-285.

Park, R. J., et al. (2003). "Sources of carbonaceous aerosols over the United States and implications for natural visibility." Journal of Geophysical Research-Atmospheres 108(D12).

Pétron, G., et al. (2014). "A New Look at Methane and Nonmethane Hydrocarbon Emissions from Oil and Natural Gas Operations in the Colorado Denver-Julesburg Basin." Journal of Geophysical Research-Atmospheres 119(11): 6836-6852.

Petzold, A., et al. (2013). "Intercomparison of a Cavity Attenuated Phase Shift-based extinction monitor (CAPS PMex) with an integrating nephelometer and a filter-based absorption monitor." Atmospheric Measurement Techniques 6(5): 1141-1151.

Ramanathan, V., et al. (2001). "Atmosphere - Aerosols, climate, and the hydrological cycle." Science 294(5549): 2119-2124.

Reddy, P. J., et al. (1995). "DEVELOPMENT OF A STATISTICAL-MODEL FOR FORECASTING EPISODES OF VISIBILITY DEGRADATION IN THE DENVER METROPOLITAN-AREA." Journal of Applied Meteorology 34(3): 616-625.

Richter, D., et al. (2015). "Compact highly sensitive multi-species airborne mid-IR spectrometer." Applied Physics B-Lasers and Optics 119(1): 119-131.

Ridley, B. A. and F. E. Grahek (1990). "A SMALL, LOW FLOW, HIGH-SENSITIVITY REACTION VESSEL FOR NO CHEMILUMINESCENCE DETECTORS." Journal of Atmospheric and Oceanic Technology 7(2): 307-311.

Rosenberg, P. D., et al. (2012). "Particle sizing calibration with refractive index correction for light scattering optical particle counters and impacts upon PCASP and CDP data collected during the Fennec campaign." Atmospheric Measurement Techniques 5(5): 1147-1163.

5   Scamehorn, H. L. (2002). High Altitude Energy: A History of Fossil Fuels in Colorado. Boulder, CO. Colorado, University Press of Colorado.

Schneider, W., et al. (1987). "ABSORPTION CROSS-SECTIONS OF NO2 IN THE UV AND VISIBLE REGION (200 - 700 NM) AT 298-K." Journal of Photochemistry and Photobiology a-Chemistry 40(2-3): 195-217.

Seinfeld, J. H. and S. N. Pandis (2006). Atmospheric chemistry and physics: from air pollution to climate change. Hoboken, New Jersey, John Wiley and Sons, Inc.

15   Slusher, D. L., et al. (2004). "A thermal dissociation–chemical ionization mass spectrometry (TD-CIMS) technique for the simultaneous measurement of peroxyacyl nitrates and dinitrogen pentoxide." Journal of Geophysical Research: Atmospheres 109.

Thornton, J. A., et al. (2000). "Atmospheric NO2: In situ laser-induced fluorescence detection at parts per trillion mixing ratios." Analytical Chemistry 72(3): 528-539.

Vu, K. T., et al. (2016). "Impacts of the Denver Cyclone on Regional Air Quality and Aerosol Formation in the Colorado Front Range during FRAPPÉ 2014 " Atmos. Chem. Phys. Discuss.

25   Warneke, C., et al. (2007) Determination of urban volatile organic compound emission ratios and comparison with an emissions database. J. Geophys. Res.- Atmos. 112, DOI: 10.1029/2006JD007930

Watson, J. G., et al. (1998). Northern Front Range Air Quality Study Final Report, Colorado State University.

30   Weber, R. J., et al. (2016). "High aerosol acidity despite declining atmospheric sulfate concentrations over the past 15 years." Nature Geoscience 9(4): 282-+.

Wolff, G. T., et al. (1981). "VISIBILITY-REDUCING SPECIES IN THE DENVER BROWN CLOUD .2. SOURCES AND TEMPORAL PATTERNS." Atmospheric Environment 15(12): 2485-2502.

Ying, Q., et al. (2004). "Source apportionment of visibility impairment using a three-dimensional source-oriented air quality model." Environmental Science & Technology 38(4): 1089-1101.

Zheng, W., et al. (2011). "Characterization of a thermal decomposition chemical ionization mass spectrometer for the measurement of peroxy acyl nitrates (PANs) in the atmosphere." Atmospheric Chemistry and Physics 11(13): 6529-6547.
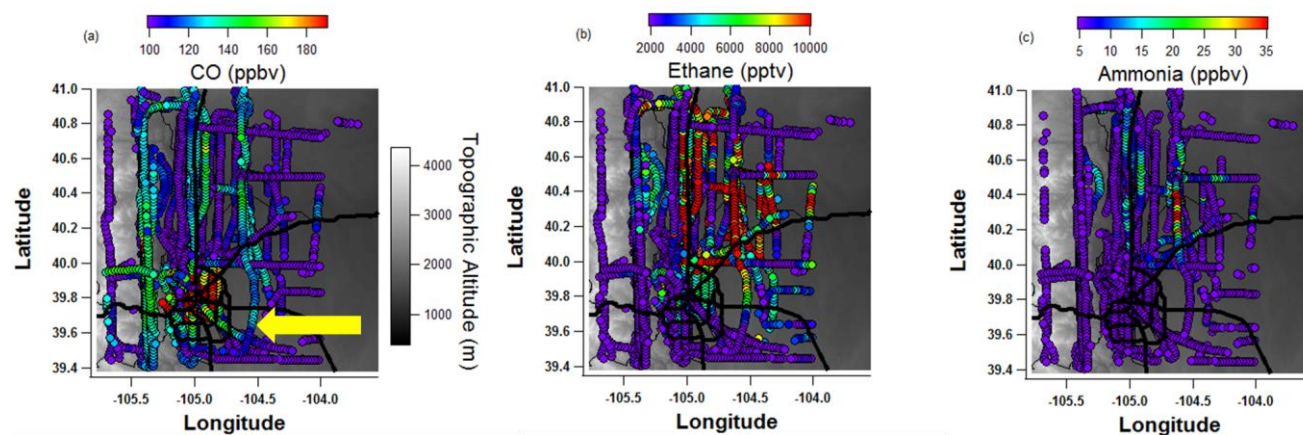
Figures

Figure 1. C-130 flight tracks in the Colorado Front Range, color coded with observed mixing ratios of (a) CO, (b) ethane, and (c) ammonia. The yellow arrow indicates the Denver metropolitan area. To the west of the Denver metropolitan area are the Rocky Mountain foothills depicted by the topographic color scheme.
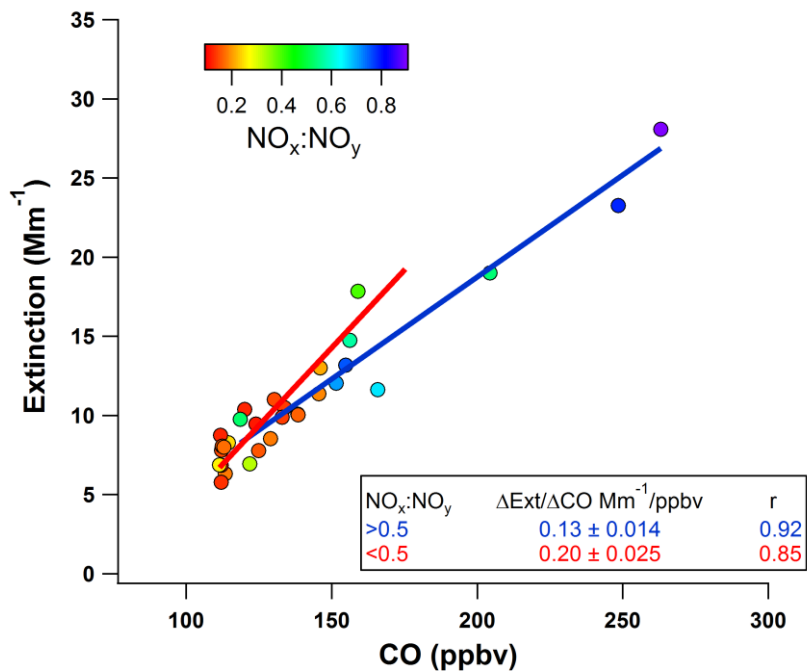
Figure 2. Orthogonal distance linear regression fits to extinction (Mm^{-1}) vs. CO (ppbv) under fresh (blue fit line) and aged air masses (red fit line).
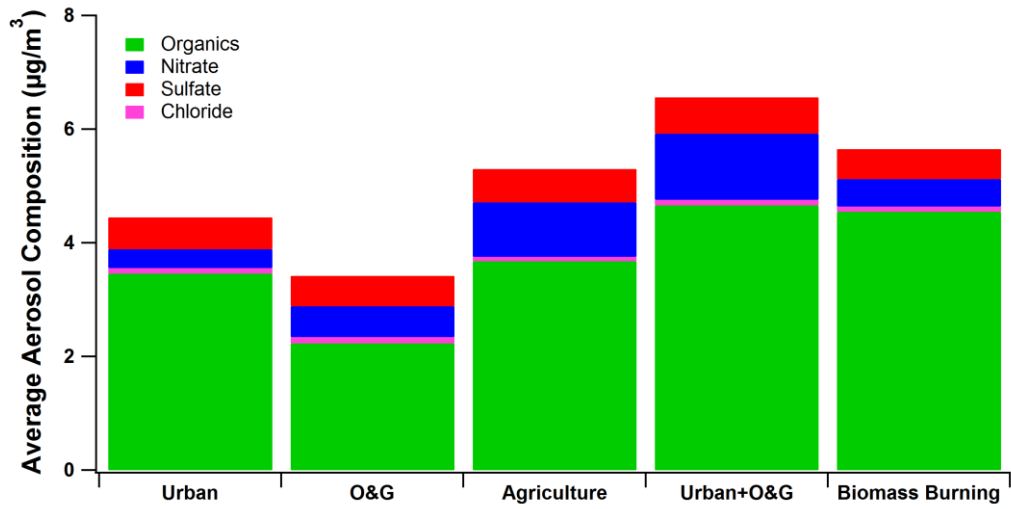
Figure 3. Average chemical composition (μg m^{-3}) of non-refractory aerosols under different air mass source.
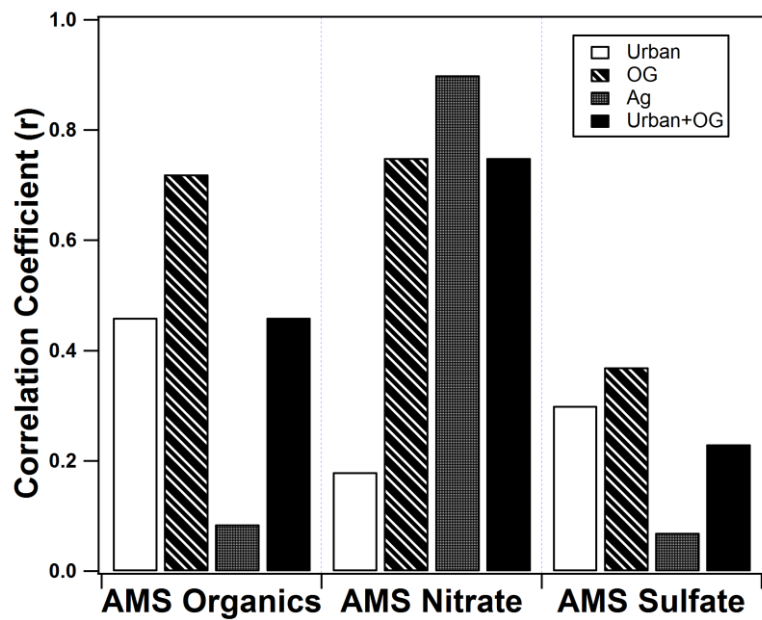
Figure 4. Correlations coefficients of β_{ext} vs. aerosol composition under urban, O&G, agriculture, urban + O&G emissions.
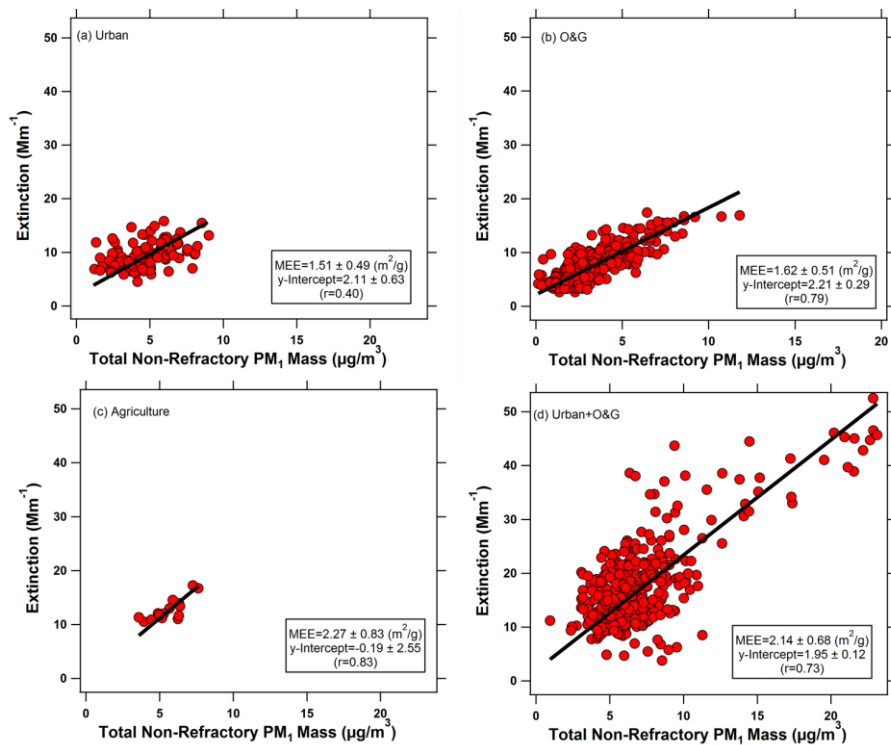
Figure 5. Mass extinction efficiencies (MEE) under (a) urban, (b) O&G, (c) agriculture, and (d) urban+O&G influence
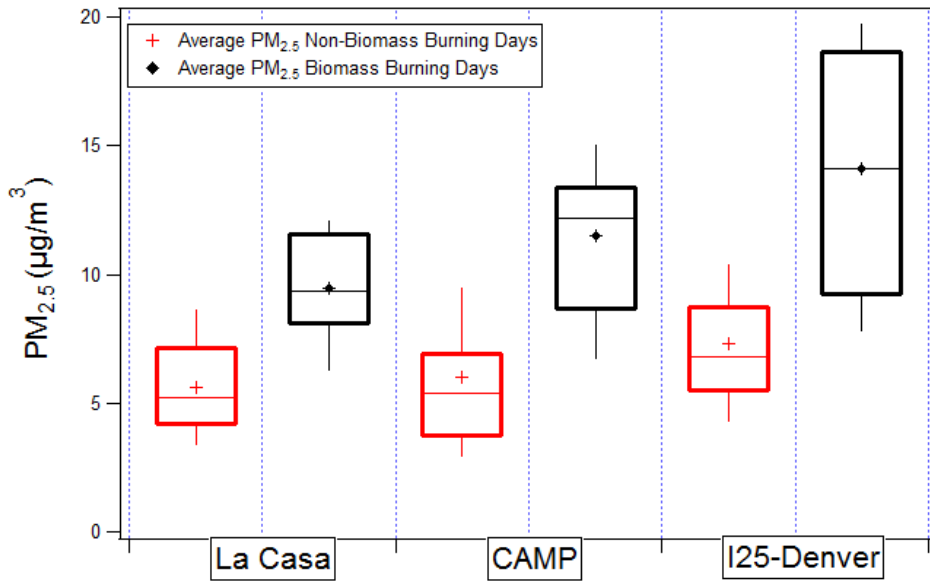
Figure 6. Daily (9 am - 7 pm local time) average PM$_{2.5}$ mass concentration for 3 monitoring sites for (a) non-biomass
5   burning days of July 26, 29, 31 and August 02, 03, 07, 08, 15, 16, 18 and (b) biomass burning days of August 11 and 12. The
whisker top, whisker bottom, box top and box bottom represents the 90th, 10th, 75th, and 25th percentiles.
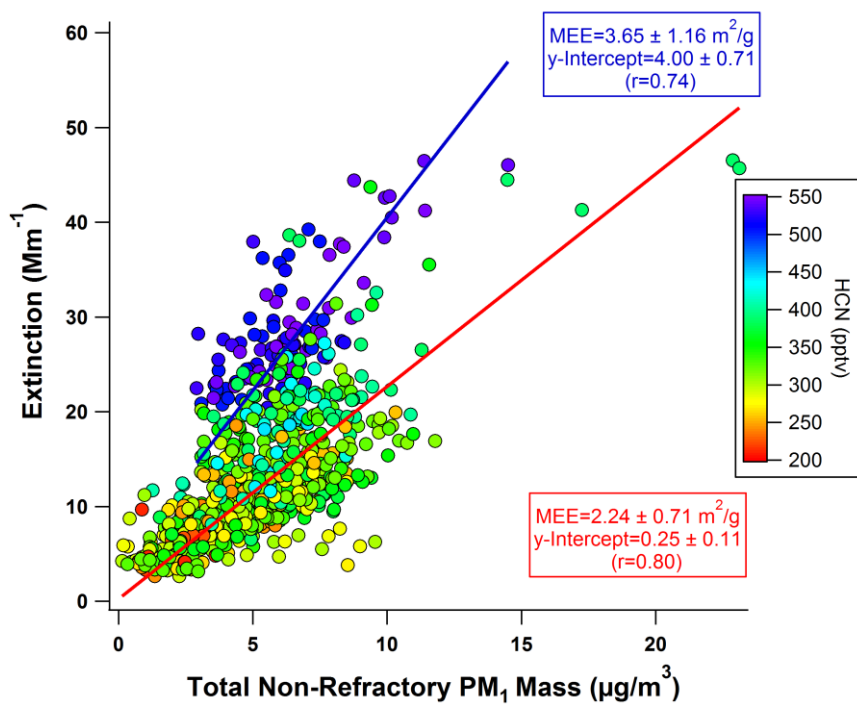
Figure 7. Orthogonal distance linear regression fits to extinction (Mm^{-1}) vs. total NR-PM$_1$ mass (μg/m^3). Data points are color coded with the average HCN mixing ratio for non-biomass burning and biomass burning days.